International Journal of Antimicrobial Agents 67 (2026) 107693

Contents lists available at ScienceDirect

International Journal of Antimicrobial Agents

journal homepage: www.elsevier.com/locate/ijantimicag

EnvZ mutation–driven downregulation of catecholate siderophore receptors and concurrent TonB complex repression confer cefiderocol resistance in a KPC-producing ST11-KL64 hypervirulent *Klebsiella pneumoniae*

Danni Pu[a,b,c,d], Xianxia Zhuo[b,c,d,e], Rongrong Song[a,b,c,d], Chunhui Wang[f], Jiankang Zhao[b,c,d,*], Bin Cao[a,b,c,d,e,*]

[a] *Graduate School of Peking Union Medical College, Chinese Academy of Medical Sciences, Peking Union Medical College, Beijing, China*
[b] *National Center for Respiratory Medicine, State Key Laboratory of Respiratory Health and Multimorbidity, National Clinical Research Center for Respiratory Diseases, Beijing, China*
[c] *Institute of Respiratory Medicine, Chinese Academy of Medical Sciences, Beijing, China*
[d] *Department of Pulmonary and Critical Care Medicine, Center of Respiratory Medicine, China-Japan Friendship Hospital, Beijing, China*
[e] *Department of Pulmonary and Critical Care Medicine, Capital Medical University, Beijing, China*
[f] *PerkinElmer Management (Shanghai) Co., Ltd, Shanghai, China*

ARTICLE INFO

Article history:
Received 11 July 2025
Accepted 14 December 2025

Editor: Dr Fupin Hu

Keywords:
Klebsiella pneumoniae
KPC
Cefiderocol
Siderophore
Iron transport system
EnvZ/OmpR
Two-component signal transduction systems

ABSTRACT

Objectives: Cefiderocol is an ultimate antibiotic option for Carbapenem-resistant hypervirulent *Klebsiella pneumoniae* (CR-hvKP). While resistance often involves metallo-β-lactamases, mechanisms in KPC-producing strains are unclear. This study aimed to elucidate novel cefiderocol resistance mechanisms in a clinical KPC-producing ST11-KL64 CR-hvKP isolate.

Methods: Cefiderocol-resistant mutants were generated through *in vitro* experimental evolution. Resistance-associated mutations were identified by whole-genome sequencing. Transcriptomic and proteomic analyses were performed to characterize global regulatory changes and were validated by qRT-PCR and targeted genetic manipulation. Additional tests examined siderophore production, intracellular iron levels, bacterial fitness, oxidative stress tolerance, and macrophage survival.

Results: All high-level cefiderocol-resistant mutants acquired a gain-of-function mutation in the sensor kinase EnvZ (V145G). Integrated transcriptomic and proteomic analyses showed that the *envZ* mutation drove marked downregulation of catecholate siderophore receptors (*cirA* and *fepA*), impairing cefiderocol uptake. In parallel, the TonB–ExbB–ExbD energy transduction complex was independently and stably downregulated, synergistically contributing to resistance. Notably, *envZ* mutation–associated repression of the enterobactin biosynthesis gene *entB* paradoxically increased cefiderocol susceptibility, indicating a regulatory trade-off. Resistant mutants exhibited reduced siderophore production, impaired intracellular iron accumulation, and significant fitness costs, including attenuated growth, reduced oxidative stress tolerance, and decreased survival within macrophages.

Conclusions: In conclusion, this work uncovers a novel cefiderocol resistance mechanism in KPC-producing ST11-KL64 CR-hvKp, initiated by the *envZ* mutation, which causes the downregulation of catecholate siderophore receptors. This receptor repression, combined with the stable downregulation of the TonB-ExbB-ExbD energy complex, severely impairs cefiderocol's "Trojan horse" active uptake. This resistance mechanism is accompanied by a fitness trade-off, providing critical insights into the evolution of these superbugs.

© 2025 Elsevier Ltd and International Society of Antimicrobial Chemotherapy. All rights are reserved, including those for text and data mining, AI training, and similar technologies.

* Corresponding authors. Mailing address: Department of Pulmonary and Critical Care Medicine, Center of Respiratory Medicine, National Clinical Research Center for Respiratory Diseases, National Center for Respiratory Medicine, China-Japan Friendship Hospital, Beijing 100029, China.
E-mail addresses: zjk4265296@163.com (J. Zhao), caobin_ben@163.com (B. Cao).

https://doi.org/10.1016/j.ijantimicag.2025.107693
0924-8579/© 2025 Elsevier Ltd and International Society of Antimicrobial Chemotherapy. All rights are reserved, including those for text and data mining, AI training, and similar technologies.

1. Introduction

Around the world, *Klebsiella pneumoniae* is a pathogen of great clinical importance as it results in severe community-acquired and hospital-acquired infections [1,2]. Numerous diseases, including liver abscesses, bloodstream infections, pneumonia, and urinary tract infections, can result from it [3]. Carbapenem-resistant *K. pneumoniae* (CRKp) has become a major risk to human health [4]. Furthermore, the hypervirulent *K. pneumoniae* (hvKp) has also been spreading at a fast pace [5]. In recent years, the KPC-2-producing ST11-KL64 hypervirulent CRKp strain (CR-hvKp) has frequently emerged in China, which exhibits high transmissibility, hyper-resistance, and hypervirulence, leaving limited therapeutic options for severe infections [6].

A new cephalosporin named cefiderocol, which is conjugated with a siderophore, gets into bacteria through an active uptake mechanism by means of the iron transport system [7]. The new antibiotic agent contains a chlorocatechol sidechain that imitates catecholate-type siderophores (e.g., enterobactin) that chelate iron, allowing it to get into bacterial cells via TonB-dependent iron transporter channels [8]. The compound shows remarkable *in vitro* activity against a wide range of carbapenem-resistant bacteria, including CR-hvKp [7]. However, when its entry pathway into bacteria is obstructed, resistance can develop. EnvZ and OmpR are the typical two-component systems (TCSs) in *K. pneumoniae*, where EnvZ acts as a sensor kinase and OmpR acts as a response regulator [9]. Microarray data from the Δ*ompR*Δ*envZ* mutant showed a marked upregulation of several Fur-regulated genes, especially those involved in enterobactin synthesis and transport [10]. Cefiderocol resistance may also arise as a result of TCS alterations. Yamano et al. [11] found that the mutations in *envZ* mutations were present in strains with an elevated MIC value for cefiderocol. Another study demonstrated that combined mutations in the KPC gene and *envZ* conferred a ≥256-fold increase in cefiderocol MIC [12]. Cefiderocol mimics the structure of the enterobactin siderophore, and the two often compete with each other during bacterial uptake. Yang et al. revealed that deletion of *entB* can reduce the cefiderocol MIC by more than eightfold [13]. Additionally, the function of the iron transporter depends on three inner membrane proteins, TonB–ExbB–ExbD, which transfer energy to the outer membrane for iron transport [8]. The mutations or downregulation in these proteins also caused resistance to cefiderocol [14]. However, investigations on these proteins are limited, further stuides is needed to elucidate the potential mechanisms of cefiderocol resistance.

A monitoring study named SIDERO-WT-2014 indicated that cefiderocol had 100% efficacy against Enterobacteriaceae that produce KPC, yet it was only 58% effective when it came to Enterobacteriaceae that produce NDM [15]. For most *K. pneumoniae*, the resistance to cefiderocol is caused by the combined influence of NDM expression and decreased expression or mutations in the siderophore receptor genes (e.g., *cirA*) [16–18]. Nevertheless, our previous research has found that KPC-producing CR-hvKp, a type of prevalent strain in China, can also develop resistance to cefiderocol [19]. Another study revealed that cefiderocol resistance in CR-hvKP can arise from *cirA* mutation combined with the co-production of KPC-2 and SHV-12 [20]. The KPC-31 variant, along with a conjugative low-copy-number vector containing the *fec* gene cluster, is another mechanism for strain resistance [21]. However, the cefiderocol resistance mechanisms in KPC-producing CR-hvKP are not fully understood.

This study, therefore, aimed to investigate novel cefiderocol resistance mechanisms in a KPC-producing CR-hvKP strain through *in vitro* laboratory evolution and multi-omics analysis.

2. Materials and methods

2.1. Bacterial isolates and antimicrobial susceptibility testing

A clinical cefiderocol-susceptible ST11-KL64 KPC-producing CR-hvKP, K27356 (MIC, 0.5 μg/ml), was employed as a parent strain to create cefiderocol-resistant *in vitro* mutants (Table S1) [22]. A VITEK-2 Compact system (bioMérieux, France) was used for antibiotic susceptibility testing (AST). The broth microdilution method in iron-depleted cation-adjusted Mueller-Hinton broth (ID-CAMHB) was used to determine the minimum inhibitory concentrations (MICs) of cefiderocol following CLSI guidelines [23]. Three duplicates of each susceptibility test were run. The CLSI 2022 standards were followed in interpreting the results [23]. The breakpoints for cefiderocol tested against *Enterobacterales* are as follows: susceptible (S), ≤4 μg/mL; intermediate (I), 8 μg/mL; and resistant (R), ≥16 μg/mL.

2.2. In vitro *evolution experiments for the selection of cefiderocol-resistant strains*

The serial passage experiments were carried out in the way that was described before [24]. Briefly, a single clone of K27356 was successively subjected to growing concentrations of cefiderocol in ID-CAMHB overnight under shaking at 37°C. The overnight cultures were moved every day into new media containing higher cefiderocol concentrations until growth was detected at 128 μg/mL (Fig. 1A). All of the cultures in the serial passage experiments were kept at -80°C for storage. One colony was randomly chosen from the final groups of three independent experiments and saved as K27356M1, K27356M2, and K27356M3 (Table S1, Fig. 1B).

2.3. Whole-genome sequencing and bioinformatics analysis

The parent strain K27356, as well as three mutant strains, K27356M1, K27356M2, and K27356M3, were sequenced using the Oxford Nanopore sequencing method on MinION flow cells. Detailed information on the parent strain K27356 can be found in our previous study [22]. Raw reads were filtered to remove low-quality sequences and adaptors using Skewer [25] and PoreChop (https://github.com/rrwick/Porechop), respectively. SPAdes Genome Assembler v3.13 [26] and Unicycler [27] were used to conduct de novo assembly 13. Prokka 1.12 [28] was utilised for gene prediction, then the gene names and products were manually corrected using UniProtKB (https://www.uniprot.org/). Species, carbapenemase, sequence type, capsular serotype, and virulent factors were annotated with Kleborate v2.3.2 [29]. With reference to the original genome of K27356, mapping and putative mutation detection were carried out using breseq v0.33.0 [30] and validated using snippy (https://github.com/tseemann/snippy). PCR and Sanger sequencing were used to confirmed the potential mutations (the primers were shown in Table S2).

2.4. Transcriptome analysis

Total RNA of the WT K27356 and cefiderocol-treated K27356M1 strains was extracted for transcriptomic analysis. In short, the overnight bacterial culture was diluted in 100 mL of MH broth at a ratio of 1:100 and was cultured until it reached the log phase. The overnight bacterial solution was centrifuged at 5,000 rpm for 10 min. Following the manufacturer's instructions, the RNeasy minikit (Qiagen) was used to extract total RNA by the enzymatic method (lysozyme) after grinding with liquid nitrogen. The Qubit 3.0 was utilised to gauge the RNA's concentration and quality. Once the extraction of RNA was up to standard, ribosomal RNA (rRNA) was

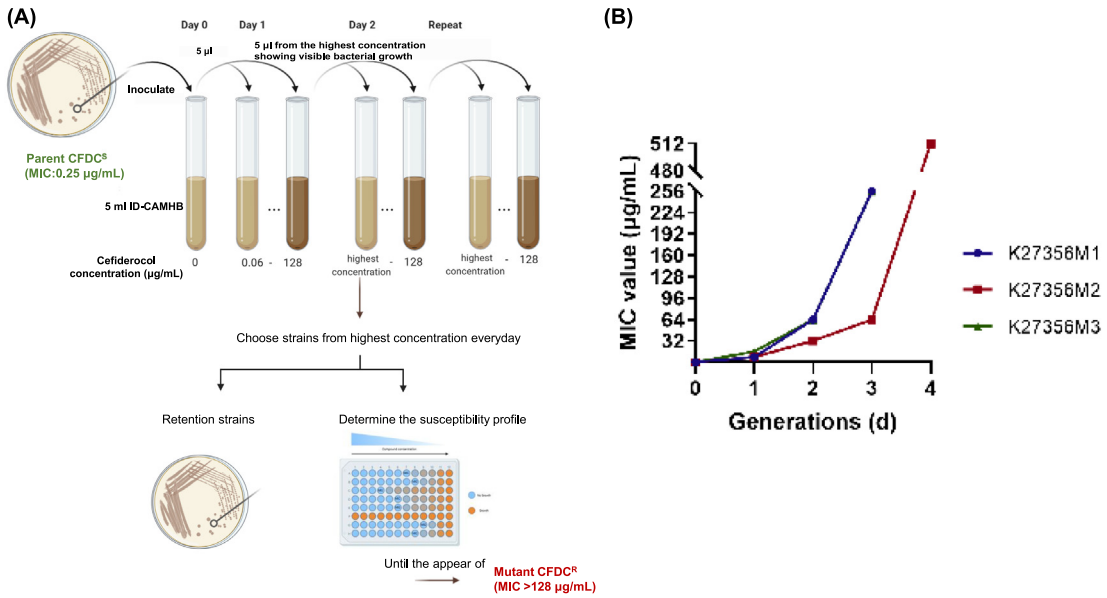

Fig. 1. Flowchart and result of the *in vitro* induction experiment. (A) Flowchart of *in vitro* evolution experiment (created with BioRender.com). Briefly, a single clone of K27356 was successively cultured in 5mL of iron-depleted cation-adjusted Mueller-Hinton broth (ID-CAMHB) containing gradually increasing concentrations of cefiderocol (0.06-128 µg/mL). Each day, 5 µL culture showing visible growth at the highest concentration was transferred to fresh ID-CAMHB containing a higher cefiderocol concentration. This process was continued until growth was detected in the tube with 128 µg/mL cefiderocol. (B) Dynamics of stepwise resistance development to cefiderocol for three experiments.

eliminated. The mRNA was then randomly broken up into short segments by enzymatic digestion. The RNA-seq reads were mapped to the genome of K27356 using Rockhopper v2.0.3 [31]. The output data were analyzed by edgeR [32]. Gene expression counts in the reference genome were calculated with the software featureCounts [33]. For the two groups, the analysis of differentially expressed genes (DEGs) was carried out by DESeq2 [34]. The clusterprofiler package (version 3) was utilised to conduct enrichment analysis on the DEGs in KEGG and GO, treating expressed genes (RPKM $>$ 1) in any samples.

2.5. Proteome analysis

To compare the proteomic profiles of WT and cefiderocol-treated *K. pneumoniae* K27356M1 strains, we performed a 4D label-free quantitative analysis coupled with LC-MS/MS, following established protocols [35,36]. The resulting tandem mass spectrometry data were processed using the MaxQuant search engine (v.1.5.2.8) [37]. Search parameters were configured for a full tryptic digest, permitting a maximum of two missed cleavages and a minimum peptide length of six amino acid residues. Mass error tolerances were set to 10 PPM for precursor ions and 0.02Da for fragment ions. A stringent false discovery rate (FDR) of 1% was applied at the protein, peptide, and peptide-spectrum match (PSM) levels, with protein identification requiring at least one unique peptide. Differentially expressed proteins (DEPs) were defined as those that exhibited a log2 fold change of $>$0.5 or $<$-0.5 with a P-value $<$ 0.05. These DEPs were subsequently subjected to GO and KEGG pathway enrichment and clustering analyses.

2.6. Quantitative real-time PCR (qRT-PCR)

A total of 1 mL of bacterial culture was used for RNA extraction for each isolate using the same method as the transcriptomic analysis mentioned above. With a total of 1 µg of RNA, the RevertAid First Strand cDNA Synthesis Kit (Thermo Fisher Scientific) was utilised to synthesise the first-strand cDNA. The QuantStudio 5 real-time PCR system (ThermoFisher Scientific) was used for qRT-PCR to measure the expression of focused genes, and its amplification conditions were as this: 50°C for 2 minutes, 95°C for 2 minutes, and 40 cycles of 95°C for 15 seconds and 60°C for 1 minute. The expression levels of the target genes were normalised to the *rpoB* gene using $\Delta\Delta C_T$ method and using the gene expressions of K23756 as references. The primers used for qRT-PCR were listed in Table S2. Three different RNA preparations were used for all amplifications.

2.7. Reconstruction of mutations, gene knockout, and overexpression

We used PCR to amplify the upstream and downstream homologous arm fragments of *envZ, envZ* (V145G), *envZ* (G145V), and *fur*. The upstream and downstream homologous arm fusion fragments were then obtained using the gene splicing by overlap extension PCR (SOE-PCR) technique and cloned to the suicide vector pDM4 with tetracycline resistance (re-modified by our laboratory) after digestion to construct pDM4-ΔenvZ, pDM4-envZ (V145G), pDM4-envZ (G145V), and pDM4-Δfur recombinant plasmids (Table S1). The plasmids were electroporated into competent *K. pneumoniae* K27356 and K27356M1 strains, respectively. We then screened the *envZ* deletion mutant strains, K27356ΔenvZ and K27356M1ΔenvZ, *fur* deletion mutant strain, K27356M1Δfur, as well as *envZ* point mutant strains, K27356envZ^{V145G} and K27356M1envZ^{G145V}, using homologous recombination technology and the tetracycline-resistant characteristics of pDM4. The reconstructed mutations were confirmed through PCR and Sanger sequencing (primers were listed in Table S2).

To clone the *fepA, cirA, entB*, and *tonB* genes into pCasPA-TCR, DNA corresponding to their open reading frames (ORFs) was amplified by PCR using primers that carried appropriate restriction enzyme sites for cloning, and then electro-transformed into K27356M1 and K27356M1envZ^{G145V} strains to over-express target genes in host bacteria (Table S1). The transformed plasmids were confirmed through PCR and Sanger sequencing (primers were listed in Table S2).

2.8. Quantitative siderophore detections

As previously mentioned, a quantitative investigation of siderophore secretion was conducted [38]. After being diluted 100 times in M9 chelated minimum media (15.6 mg of the iron chelator 2,2-dipyridyl per 500 mL) and supplemented with 1.5 g of casamino acids (c-M9-CA) per 500 mL, bacterial cultures were brought to 0.5 McFarland standard turbidity in 0.9% (w/v) aqueous NaCl solution [39]. The strains were cultivated for a period of 24 hours under the conditions of 37°C and with a shaking speed of 130 rpm. After collecting 1.5 mL of bacterial cultures, they were centrifuged at 4300 g for 20 minutes. The supernatant containing siderophore was then transferred in triplicate to a 96-well microtiter plate filled with 100 µL of chrome azurol S (CAS) shuttle solution (composition reference [40]). When incubated in the dark at room temperature for 40 minutes, the OD 630 was measured. The assay was carried out in triplicate, with the results presented as means ± standard deviations (SD).

2.9. Single-cell inductively coupled plasma mass spectrometry (SC-ICP-MS) analysis

Strains were incubated in LB broth and c-M9-CA medium (Fe chelator) +/− addition of exogenous 1 mM $FeCl_3$ at 37°C with shaking at 180 rpm for 18h, respectively. Subsequently, the bacterial cell samples were then diluted with 1% phosphate-buffered saline (PBS) to reach a final concentration of 100,000 cells/mL, and then were made to undergo SC-ICP-MS analysis. A NexION 5000 ICP-MS system (Perkin Elmer, Waltham, MA) was used to measure the samples' total ^{56}Fe concentration. For each sample, three replicates were carried out in the SC-ICP-MS measurements with a dwell time of 50 µs and a total acquisition time of 100 seconds. The sample volume used in each analysis was 100 µL. A reaction cell using pure ammonia gas was used to remove interference from ArO^+ on $^{56}Fe^+$. Detailed SC-ICP-MS operating conditions are summarised in Table S3. Fe ion standard solutions (1, 2, and 5 ppb) prepared in 1% PBS for matching the sample matrix were used for calibration. To guarantee consistency, all standards and samples were analyzed under the same conditions.

2.10. Arnow assay

As previously mentioned, the Arnow test was used to quantify the catechol production [41]. In brief, the strains were cultured overnight in c-M9-CA medium, and the OD_{600} was measured. After that, 0.2 µM filters were used to filter the supernatants to remove any bacteria. Catechol was quantified by combining equal volumes of the sample, 0.5 N HCl, 1 N NaOH, and nitrite-molybdate reagent (consisting of 10% [wt/vol] sodium nitrate and sodium molybdate). After that, the blend was left to incubate for 5 minutes to finalise the reaction. A known concentration of 2,3-dihydroxybenzoic acid (2,3-DHBA) was used as a standard to measure absorbance at 510 nm using uninoculated media as a blank. The sample was normalised to the OD600 value of each culture to account for bacterial growth.

2.11. Relative competition assay in vitro

The relative competition *in vitro* was assessed as described [42]. Mutant cefiderocol-resistant strain K27356M1 and parental strain K27356 were cultured either separately or in a 1:1 mixture in Mueller-Hinton broth adjusted for cations and depleted of iron. At 0, 24, 48, and 72 hours, each culture was serially diluted 10-fold and then plated on LB plates with or without 16 µg/mL cefiderocol, followed by incubation at 37°C for 24 hours. The following method was used to calculate the competitive indexes (CIs): The ratio of the initial inocula was divided by the ratio of resistant CFU to susceptible CFU, and a competitive index of 1 indicates that there is no change in the competing ability of either strain.

2.12. Growth kinetics

Growth curves for all strains were measured in the following way: the logarithmic-phase bacterial culture was diluted 100-fold in LB broth with/without 0.5 mM H_2O_2, and c-M9-CA medium (Fe chelator) +/− addition of exogenous 1 mM $FeCl_3$. Three aliquots of 200 µl per dilution were transferred into a 96-well microtiter plate and covered with paraffin oil. The samples were placed in a Multiskan GO Microplate Reader (Thermo Fisher Scientific) for incubation at 37°C and agitation prior to measurement. Each culture's optical density at 600 nm (OD600) was measured at 30-minute intervals, and the plate was shaken for 15 seconds prior to each measurement. Growth curve parameters such as the time of maximum growth rate, the lag period, and the doubling time of strains in the logarithmic phase were estimated.

2.13. Phagocytosis experiment

The mouse macrophage cell line RAW 264.7 was used in the phagocytosis experiment. RAW 264.7, the mouse macrophage cell line, was cultivated in Dulbecco's modified Eagle medium (DMEM; ThermoFisher, Beijing, China) containing 10% inactivated fetal bovine serum (FBS; Invitrogen) and kept at 37°C with 5% CO_2 for 16 hours before being co-incubated with bacteria. A volume of 1 mL of fresh medium containing 5×10^5 cells per well was plated in 24-well plates and cultured until it reached 70-80% confluence prior to the addition of bacteria at a multiplicity of infection (MOI) of 100:1. The bacteria and cells were incubated together for a set period at 37°C in an environment with 5% CO_2. Wells were washed three times with PBS, which contains tetracycline (50 µg/mL), to remove the unattached bacteria. Then PBS with 0.2% Triton-X100 was added, and the mixture was incubated for 30 minutes at 37°C in an environment with 5% CO_2 for cell lysis. The lysis suspension was plated on an LB agar plate to quantify the number of ingested and surviving bacteria, and then the plates were cultured at 35°C with 5% CO_2 for 18 hours. The evaluation of the macrophage's ability to ingest was carried out through different co-incubation periods of 0, 1, 2, 4, and 6 hours. The capacity of bacteria to survive within macrophages was determined by varying the incubation time before lysis, specifically at 0, 1, 2, 4, and 6 hours. At each interval, PBS was used to gently wash the wells three times. The lysis suspension was plated on an LB agar plate to quantify the amounts of intracellular bacteria, and then the plates were cultured at 35°C with 5% CO_2 for 18 hours.

2.14. Phagocytosis observed by confocal laser scanning microscopy (CLSM)

Confocal Laser Scanning Microscopy (CLSM) was also used to observe the phagocytosis as previously described, with a few alterations [43]. The RAW264.7 cells were seeded at 5×10^5 cells/well in 1 mL DMEM medium with 10% FBS on a 20-mm glass-bottom cell culture dish (NEST), and then cultured for 16 hours at 37°C in an environment with 5% CO_2. For 2 hours, the strains infected the cells in 1 mL of DMEM medium, which contained 10% FBS and had an MOI of 100. In order to get rid of the extracellular bacteria, the cells were incubated for 30 minutes in DMEM containing 50 µg/mL tetracycline. After that, the cells were made to be stationary in 4% paraformaldehyde at room temperature for 15 min and then permeabilised with 0.2% Triton X-100 in PBS for 20 min. Then add 0.1% BSA to block at 37°C for 1 hour. Finally, the cells

Table 1
Mutations in the cefiderocol-induced resistant strains.

Strains	Position	Mutation[a]	Amino acid	Gene	Product
K27356M1	369,818	G**T**G→G**G**G	V145G	*envZ*	Osmolarity sensor protein
K27356M2	369,818	G**T**G→G**G**G	V145G	*envZ*	Osmolarity sensor protein
	3,540,737	G**T**C→G**G**C	V295G	*baeS*	Signal transduction histidine–protein kinase
K27356M3	369,818	G**T**G→G**G**G	V145G	*envZ*	Osmolarity sensor protein

[a] Bold characters represent mutated nucleotide.

were placed in incubation at 4°C overnight with anti-*K. pneumoniae* antibody (Thermo Fisher Scientific, Cleveland, OH, USA, cat# PA1-7226) and anti-F4/80 antibody (Abcam, Cambridge, MA, cat# ab6640), followed by incubation for 1 hour with an Alexa Fluor 488 conjugated secondary antibody anti-rabbit or anti-rat IgG and 40,6-diamidino-2-phenylindole (DAPI; 1 mg/mL).

2.15. Statistical analysis

The R package "statmod" [44] was utilised to test for statistically significant differences in growth kinetics.. Student's *t*-test was employed to check the expression difference between the two groups. A *P-value* of 0.05 or less was defined as significant. All experiments were carried out with three replicates.

3. Results

3.1. Mutations detected in cefiderocol-induced resistant K. pneumoniae strains

To explore the potential resistance mechanisms in *K. pneumoniae* to cefiderocol, we performed three independent replicates of the *in vitro* evolution experiments in which we exposed a previously reported clinical strain, *K. pneumoniae* K27356, to sub-lethal concentrations of cefiderocol (Fig. 1A). After increasing the cefiderocol concentration for two or three rounds of passages, we obtained three cefiderocol-resistant *K. pneumoniae* strains, denoted as K27356M1, K27356M2, and K27356M3 (Fig. 1B). The results showed that the MICs of M1 and M3 were 256 μg/mL, whereas M2 reached 512 μg/mL. WGS of these mutants, compared with the parental strain K27356, revealed the corresponding mutations. Mutations in *envZ* (V145G) were detected in all three cefiderocol-induced resistant strains, highlighting the critical role of this mutation in mediating resistance. In addition, a *baeS* (V295G) mutation, previously reported to be associated with cefiderocol resistance [24], was identified in K27356M2 (Table 1). This strain exhibited a higher cefiderocol MIC (512 μg/mL), suggesting a possible synergistic interaction between *baeS* and *envZ* mutation.

We then constructed the mutations *envZ* (V145G) and *envZ* (G145V) in the genome of the parental strain K27356 and mutant strain K27356M1 by employing genetic engineering, respectively. The obtained mutants allowed us to investigate the impact of a single mutation on cefiderocol susceptibility. Antimicrobial susceptibility testing showed an 8-fold decrease in the MIC of cefiderocol for strain K27356M1envZ^{G145V} and an 8-fold increase in strain K27356envZ^{V145G}. To clarify the influence of mutations on *envZ* function, we knocked out the gene *envZ* of both K27356 and K27356M1. Cefiderocol MICs decreased from 0.5 to 0.125 μg/mL in K27356ΔenvZ and from 256 to 16 μg/mL in K27356M1ΔenvZ (Table 2). These results indicated that the mutation in *envZ* was a gain-of-function. Furthermore, in addition to the *envZ* mutation, cefiderocol-induced resistant bacteria may have unknown genetic or epigenetic determinants of resistance. Cefiderocol resistance increases as a result of these unknown factors.

Furthermore, in order to explore the effect of mutation on the susceptibility of other antibiotics, we tested the MICs of ceftazidime, cefepime, imipenem, meropenem, tigecycline, colistin, and amikacin against cefiderocol-induced-resistant strains and *envZ* mutants. However, except for tigecycline, which showed reduced susceptibility in K27356M1, there were no obvious susceptibility alterations for other strains compared with wild-type (WT) K27356 (Table 2).

3.2. Transcriptome and proteome analysis of Cefiderocol-treated Klebsiella pneumonia

To identify the internal mechanism underlying the resistance and physiological variations of strains treated with cefiderocol, we compared the transcriptome and proteome of K27356M1 with the WT K27356.

After data filtering (log2 (fold change) $\geq$ 1 and FDR $\leq$ 0.01), a total of 142 DEGs (111 up-regulated and 31 down-regulated) were screened out in cefiderocol-treated strains when compared to the WT strain (Fig. 2A). Among them, the downexpression of genes related to iron transport (e.g., *cirA, entB, entC, fhuA, cjrC, exbB, fepA,* and *fecA*), and *cysA* was first confirmed through qRT-PCR (Figure S1). The functions of the 142 DEGs were analyzed by GO tools and categorised into different enriched functional groups; the top 10 significantly enriched terms include siderophore biosynthetic process, bacteriocin transport, lactone biosynthetic process, intracellular iron ion homeostasis, siderophore metabolic process, catechol-containing compound metabolic process, antibiotic metabolic process, tryptophan metabolic process, indolalkylamine metabolic process, and phenol-containing compound metabolic process (Figure 2B). The 142 DEGs were also subjected to KEGG pathway enrichment analysis and enriched in 67 KEGG pathways, including biosynthesis of secondary metabolites, ABC transporters, biosynthesis of amino acids, biosynthesis of siderophore group nonribosomal peptides, and biosynthesis of phenylalanine, tyrosine, tryptophan, and arginine (Fig. 2C). The proteomic responses of K27356M1 were analyzed by 4D label-free and a combined LC-MS/MS quantitative proteomic approach. A total of 327 DEPs (122 up-regulated and 205 down-regulated) were observed in cefiderocol-treated strains after data filtering (fold change $\geq$ 1.5 or $\leq$ 0.067, P $\leq$ 0.05, FDR $\leq$ 0.01) when compared to the WT strain (Fig. 3A). KEGG analysis revealed that the DEGs were predominantly associated with transport, membrane components, and various transporter activities (Figure 3B). Consistently, the GO analysis was mainly enriched in Cationic antimicrobial peptide (CAMP) resistance pathway, sulfur metabolism, two−component system, and ABC transporters (Fig. 3C).

Transcriptome and proteome analysis revealed a broad downregulation of genes and proteins involved in iron acquisition (Fig. 2A, 3A, and Table 3). Specifically, we observed a significant reduction in the expression of the entire enterobactin biosynthesis pathway (*entABCEF*). Furthermore, multiple outer membrane receptors were repressed, including key catecholate siderophore receptors (*fepA, cirA, fiu*), as well as receptors for citrate-type siderophores (*fhuA, fecA, iutA*). Crucially, the core components of the energy-transducing TonB-ExbB-ExbD system (*tonB, exbB, exbD*) were themselves among the most significantly downregulated both in transcriptome and proteome, indicating a systemic shutdown of

Table 2
Antimicrobial susceptibility result (MICs, μg/mL) [a] of cefiderocol induced-resistant strains and recombinant strains.

Strains	VITEK-2 system								Broth dilution
	CAZ	FEP	IPM	MEM	TGC	CST	AK	CIP	CFDC
K27356	**≥64**	**≥32**	**≥16**	**≥16**	2	≤ 0.5	**≥64**	**≥4**	0.5
K27356M1	**≥64**	**≥32**	**≥16**	**≥16**	≤ 0.5	≤ 0.5	**≥64**	**≥4**	**256**
K27356M2	**≥64**	**≥32**	**≥16**	**≥16**	1	≤ 0.5	**≥64**	**≥4**	**512**
K27356M3	**≥64**	**≥32**	**≥16**	**≥16**	≤ 0.5	≤ 0.5	**≥64**	**≥4**	**256**
K27356M1envZ^{G145V}	**≥64**	**≥32**	**≥16**	**≥16**	1	≤ 0.5	**≥64**	**≥4**	**32**
K27356M1ΔenvZ	**≥64**	**≥32**	**≥16**	**≥16**	1	≤ 0.5	**≥64**	**≥4**	**16**
K27356envZ^{V145G}	**≥64**	**≥32**	**≥16**	**≥16**	2	≤ 0.5	**≥64**	**≥4**	4
K27356ΔenvZ	**≥64**	**≥32**	**≥16**	**≥16**	1	≤ 0.5	**≥64**	**≥4**	0.125
K27356M1Δfur	**≥64**	**≥32**	**≥16**	**≥16**	0.5	≤ 0.5	**≥64**	**≥4**	**64**
K27356M1::pCasPA-cirA	**≥64**	**≥32**	**≥16**	**≥16**	0.5	≤ 0.5	**≥64**	**≥4**	**128**
K27356M1:: pCasPA-fepA	**≥64**	**≥32**	**≥16**	**≥16**	0.5	≤ 0.5	**≥64**	**≥4**	**64**
K27356M1::pCasPA-entB	**≥64**	**≥32**	**≥16**	**≥16**	≤ 0.5	≤ 0.5	**≥64**	**≥4**	**512**
K27356M1::pCasPA-tonB	**≥64**	**≥32**	**≥16**	**≥16**	0.5	≤ 0.5	**≥64**	**≥4**	**32**
K27356M1envZ^{G145V}::pCasPA-tonB	**≥64**	**≥32**	**≥16**	**≥16**	1	≤ 0.5	**≥64**	**≥4**	2
K27356M1::pCasPA	**≥64**	**≥32**	**≥16**	**≥16**	≤ 0.5	≤ 0.5	**≥64**	**≥4**	**256**

[a] CAZ, ceftazidime; FEP, cefepime; IPM, imipenem; MEM, meropenem; TGC, tigecycline; CST, colistin; AK, amikacin; CFDC, cefiderocol. Numbers shown in bold were resistance judged by CLSI breakpoint.

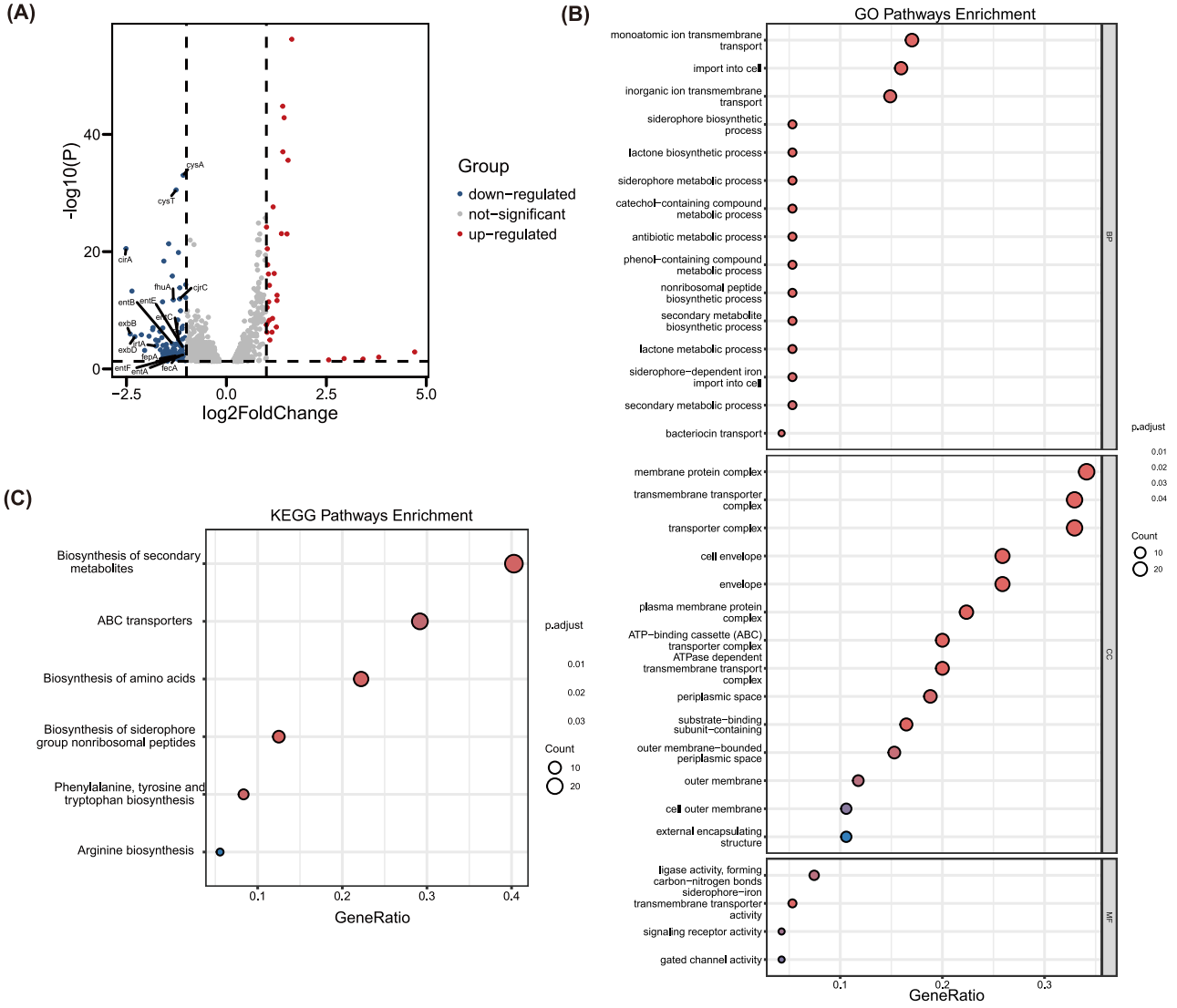

Fig. 2. Transcriptomic analysis between K27356 and K27356M1. (A) The volcano plot of DEGs, the red dots were up-regulated genes, and the blue dots were down-regulated genes; genes related to iron transfer systems and the *cysAT* were marked in black. (B) The top 6 KEGG enrichment pathways for DEGs, the rich factor refers to the ratio of the number of DEGs in the pathway and the number of all annotated genes in the pathway. (C) GO enrichment analysis of differentially expressed genes.

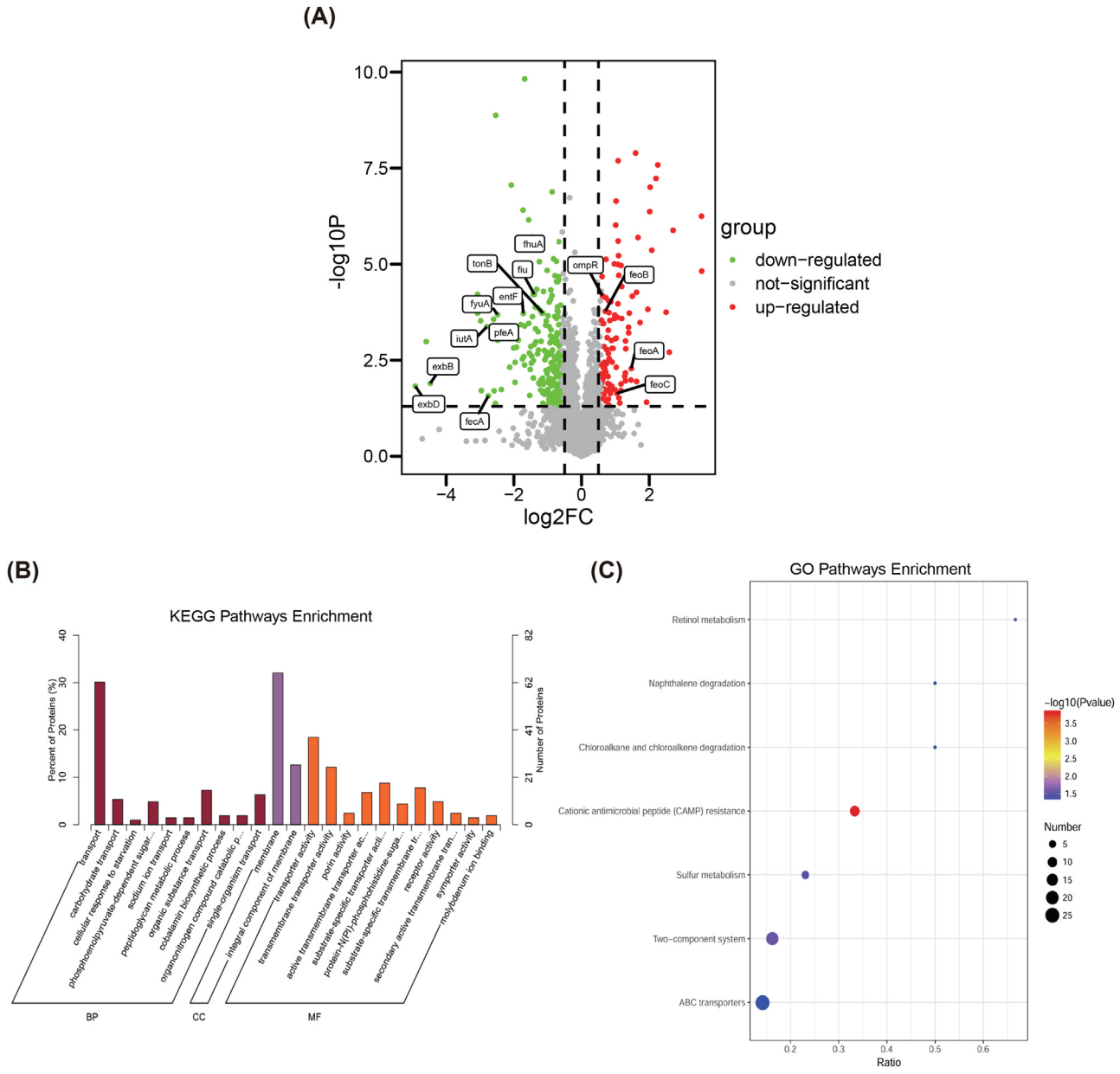

Fig. 3. Proteome analysis between K27356 and K27356M1. (A) The volcano plot of DEPs, the red dots were up-regulated genes, and the green dots were down-regulated genes; genes related to iron transfer systems were marked. (B) KEGG enrichment pathways for DEPs, the rich factor refers to the ratio of the number of DEPs in the pathway and the number of all annotated proteins in the pathway. (C) GO enrichment analysis of differentially expressed proteins.

TonB-dependent transport. In contrast, the *ferrous* iron transport system (*feoABC*) and TCS response regulator *ompR* were upregulated at the protein level. Furthermore, we also noticed that *cysAT* (sulfate/thiosulfate import-related component of the ABC transporter complex) was downregulated in K27356M1.

By comparing the Transcriptome-Proteome analysis, there are only 31 overlapping differentially expressed genes and proteins (Fig. 4A, B). As shown in Fig. 4A, the correlation coefficient of the expressions of protein and gene was 0.058, indicating that the expression of proteins and genes was not always consistent [45]. 27 down-regulated and 2 up-regulated genes were found among the 31 common DEGs and DEPs, and 2 genes were up-regulated in the proteome but down-regulated in the transcriptome (Fig. 4B). Among them, we noticed that *cirA, fepA, exbB, and exbD*, the key genes that regulate the active entry of cefiderocol into bacteria, were both down-regulated in transcriptome and proteome analysis. KEGG analysis showed that the DEGs and DEPs were mainly involved in CAMP resistance, ABC transporters, phosphotransferase system (PTS), biosynthesis of siderophore group, and two−component system (Fi. 4C). GO functional enrichment analysis of the proteome and transcriptome was plotted (Fig. 4D). DEGs and DEPs were mainly associated with transport, transporter activity, oxidoreductase activity, unfolded protein binding, sigma factor activity, and membrane.

3.3. EnvZ mutation–driven downregulation of catecholate siderophore receptors and concurrent TonB complex repression is associated with increased cefiderocol MIC

To precisely define the regulatory role of the *envZ* mutation, we first set out to investigate the effects of *envZ*(V145G) on the enterobactin biosynthesis genes (*entB*), TonB-dependent

Table 3
Differentially expressed genes and proteins associated with iron transmembrane transport in K27356M1 compared with KP27356.

Gene ID/Protein ID	Genes	Products	log2 fold change	*P*-value
Differentially expressed genes				
ONIDOABA_00721	*exbB*	Biopolymer transport protein ExbB	-2.40507	3.07E-08
ONIDOABA_00722	*exbD*	Biopolymer transport protein ExbD	-2.28827	9.51E-08
ONIDOABA_01671	*cirA*	Colicin I receptor	-2.51068	1.03E-23
ONIDOABA_03237	*fhuA*	Ferrichrome outer membrane transporter/phage receptor	-1.32725	1.65E-14
ONIDOABA_03397	*irtA*	Iron import ATP-binding/permease protein IrtA	-1.76398	5.90E-06
ONIDOABA_03882	*entA*	2,3-dihydro-2,3-dihydroxybenzoate dehydrogenase	-1.15164	0.000714
ONIDOABA_03883	*entB*	Enterobactin synthase component B	-1.35471	2.02E-06
ONIDOABA_03884	*entE*	Enterobactin synthase component E	-1.08404	1.20E-05
ONIDOABA_03891	*entF*	Enterobactin synthase component F	-1.06079	0.000360
ONIDOABA_03885	*entC*	Isochorismate synthase EntC	-1.19260	4.32E-07
ONIDOABA_03894	*fepA*	Ferrienterobactin receptor	-1.21197	0.000431
ONIDOABA_04094	*fecA*	Fe (3+) dicitrate transport protein FecA	-1.14636	1.58E-12
ONIDOABA_05571	*cjrC*	Colicin Js-sensitive receptor protein	-1.09515	1.13E-12
ONIDOABA_01492	*cysA*	Sulfate/thiosulfate import ATP-binding protein CysA	-1.02249	9.64E-37
ONIDOABA_01490	*cysT*	Sulfate transport system permease protein CysT	-1.25730	3.55E-34
Differentially expressed proteins				
AEW60685.1	*iutA*	Putative TonB-dependent receptor	-2.79835	0.000427
AEW60842.1	*pfeA*	TonB dependent outer membrane siderophore receptor protein	-2.05554	0.000407
AEW62354.1	*cirA*	Colicin I receptor	-2.75286	0.026680
AEW61578.1	*fecA*	Putative tonB-dependent receptor	-1.86907	0.000950
AEW61876.1	*tonB*	Transport protein TonB	-1.13853	0.000189
AEW62169.1	*fyuA*	Pesticin_yersiniabactin TonB-dependent receptor	-2.48110	0.000207
AEW63250.1	*exbD*	Biopolymer transport protein ExbD	-4.91224	0.014985
AEW63251.1	*exbB*	TonB-system energiser ExbB	-4.46972	0.012661
AEW60685.1	*iutA*	Putative TonB-dependent receptor	-2.79835	0.000427
AEW60848.1	*fiu*	Catecholate siderophore receptor Fiu	-1.39238	6.16E-05
AEW62012.1	*fhuA*	Iron complex outermembrane recepter protein	-1.44293	1.99E-06
AEW62164.1	*entF*	Enterobactin synthetase component F	-1.72006	0.000194
AEW63625.1	*ompR*	Osmolarity response regulator	0.61810	6.66E-05
AEW63628.1	*feoA*	Ferrous iron transport protein A	1.47044	0.005237
AEW63629.1	*feoB*	Ferrous iron transport protein B	0.70141	0.000169
AEW63630.1	*feoC*	Putative Ferrous Iron Transport Protein C (Feoc)	1.04165	0.023011

receptors (*cirA, cjrC, fepA, fecA*), and the TonB-ExbB-ExbD complex (*exbB*) (Figure S2). In the K27356M1 background, their transcript levels went down compared with K27356. As expected, in the K27356M1envZ^{G145V} background, reversion of *envZ* successfully restored the expression of TonB-dependent receptor genes—particularly the catecholate siderophore receptors involved in cefiderocol uptake (*fepA* and *cirA*)—as well as the enterobactin biosynthesis gene *entB*, to levels comparable with the WT strain. Intriguingly, however, the expression of the TonB-ExbB-ExbD complex gene *exbB* remained significantly downregulated, even after the *envZ* mutation was corrected. This finding suggests that while the *envZ* mutation is the primary driver for repressing enterobactin synthesis and siderophore receptors [10], the shutdown of the TonB energy-transducing system represents a stabilised, downstream adaptation that is not directly reversible by restoring *envZ* alone.

Given the low expression levels of iron import–related genes, among which catecholate siderophore receptors (*fepA, cirA*) and the TonB-ExbB-ExbD complex were both downregulated in transcriptome and proteome analysis, and considering that these genes are also key mediators of cefiderocol entry, we next examined their impact on cefiderocol susceptibility. We then complemented K27356M1 with plasmids overexpressing the *cirA, fepA, tonB,* and *entB* genes, K27356M1envZ^{G145V} with a plasmid overexpressing the *tonB* gene. The cefiderocol MICs of K27356M1 strains with over-expression for pCasPA-cirA, or pCasPA-fepA, reduced two- to four-fold. When the pCasPA-tonB plasmid was complemented, the MIC of K27356M1 even decreased to 32 μg/mL. Furthermore, K27356M1envZ^{G145V}, in which we complemented pCasPA-tonB, further restored susceptibility to cefiderocol (2 μg/mL). Cefiderocol and enterobactin share the same entry pathway into bacteria and therefore compete with each other [13]. As a result, the cefiderocol MIC of K27356M1 with pCasPA-entB increased to 512 μg/mL (Table 2).

Although no changes in *fur* expression were detected at either the transcriptomic or proteomic level in K27356M1, the activating mutation in *envZ* may enhance Fe^{2+} transport and elevate intracellular iron levels, thereby activating *fur*, which in turn represses the expression of the aforementioned Fe^{3+} uptake–related genes [9]. Therefore, we also examined whether deletion of *fur* would produce a similar effect to *envZ*. The AST result of K27356M1Δfur was consistent with our hypothesis, showing a fourfold decrease in the MIC after *fur* deletion.

These results indicated that the downregulation of the catecholate siderophore receptors caused by the mutation in *envZ*, an effect that can also be reproduced by *fur* deletion, together with suppression of the TonB-ExbB-ExbD complex, contributes to reduced susceptibility to cefiderocol. In contrast, downregulation of enterobactin biosynthesis genes may enhance bacterial susceptibility to cefiderocol.

3.4. Cefiderocol-resistant strain exhibits a reduced ability to produce catecholate-type siderophores and acquire iron

Depending on how cefiderocol reaches the bacterium, changes in the outer membrane transport system may result in strains that are resistant to it [8]. Therefore, we examined whether the K27356M1 strain exhibited impaired iron acquisition capability. We used the SideroTec Assay to quantitatively detect the siderophore. The average concentration of siderophore produced by mutant strain K27356M1 was 16.07 μg/mL, while that by parent strain K27356 was 26.23 μg/mL (Fig. 5A). A significant difference was observed between them ($P < 0.05$). The Arnow assay showed that K27356M1 had lower catechol production (an average of

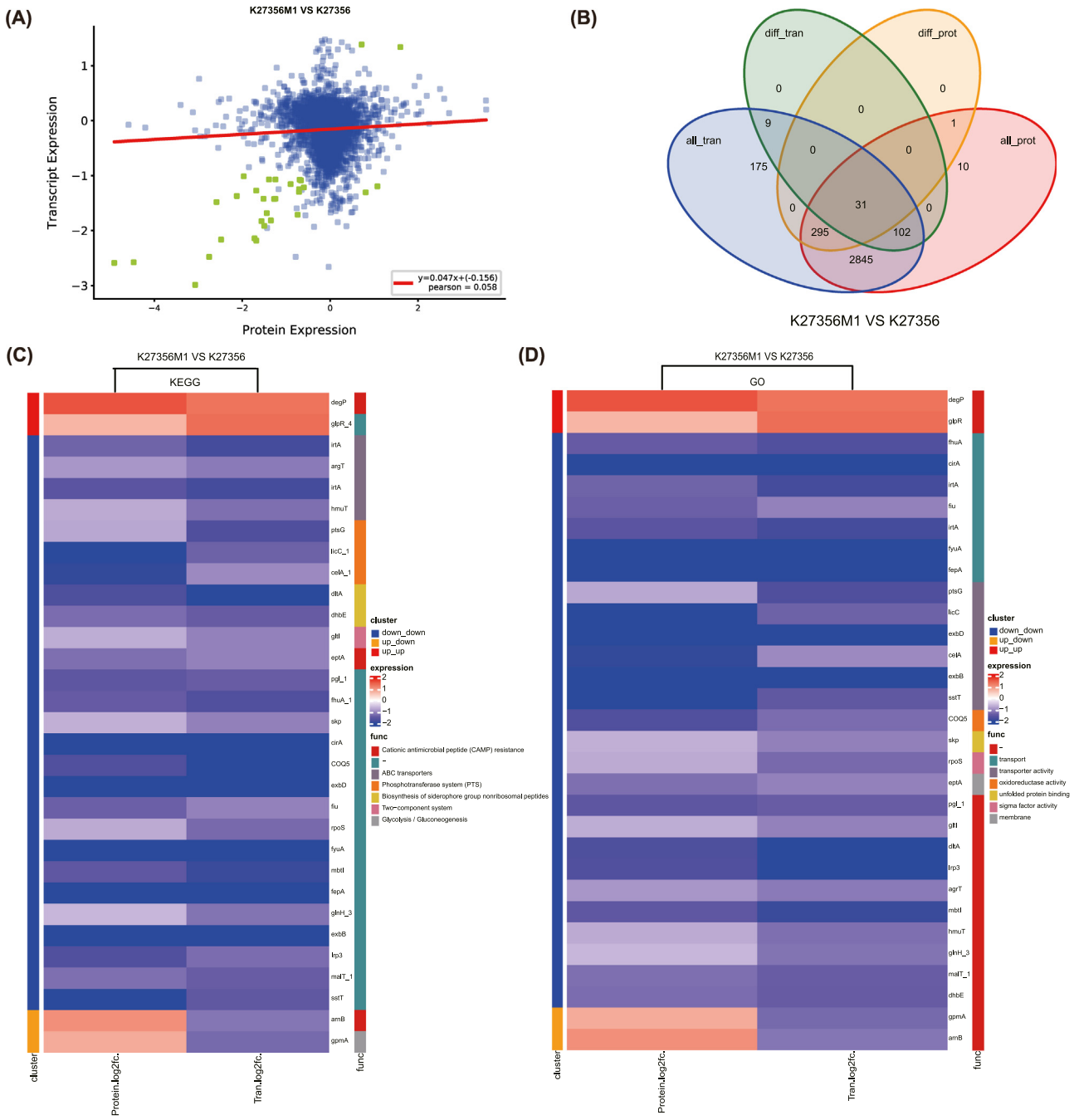

Fig. 4. Integration analysis of proteome and transcriptome. (A) Scatter plot of genes and their corresponding protein expression in the cefiderocol-treated strain vs. the WT strain. BU, transcript level, and protein level were both up-regulated. (B) Venn diagram of the number of DEPs and DEGs in proteomics and transcriptome. (C) KEGG analysis of the DEGs shared by the proteome and transcriptome. (D) GO analysis of the DEGs shared by proteome and transcriptome.

7.3 μg/mL) than K27356 (an average of 12.74 μg/mL) ($P < 0.01$) (Fig. 5A).

We further compared the intracellular concentration of iron in the two bacterial strains using SC-ICP-MS. As depicted in Fig. 5B, K27356M1 showed significantly lower levels of iron than the WT strain both in LB medium (3868.96 ag vs. 4755.29 ag, $P < 0.05$) and in iron limitation conditions (1272.31 ag vs. 2472.69 ag, $P < 0.01$), while there is no significant difference between the two strains following exogenous iron supplementation. These results may also indicate that the presence of free inorganic iron is associated with reduced susceptibility to cefiderocol.

3.5. Reduced bacterial fitness as a consequence of cefiderocol resistance

Given that iron is an essential element for biological processes in pathogenic bacteria [46], we sought to investigate whether the impaired iron acquisition capacity of K27356M1 would compromise bacterial fitness. The strains' fundamental biological changes prior to and following cefiderocol induction were then contrasted, including the growth curve under varying iron availability conditions and *in vitro* competitiveness. The cefiderocol-treated strain exhibited a slower growth rate as compared to the WT strain,

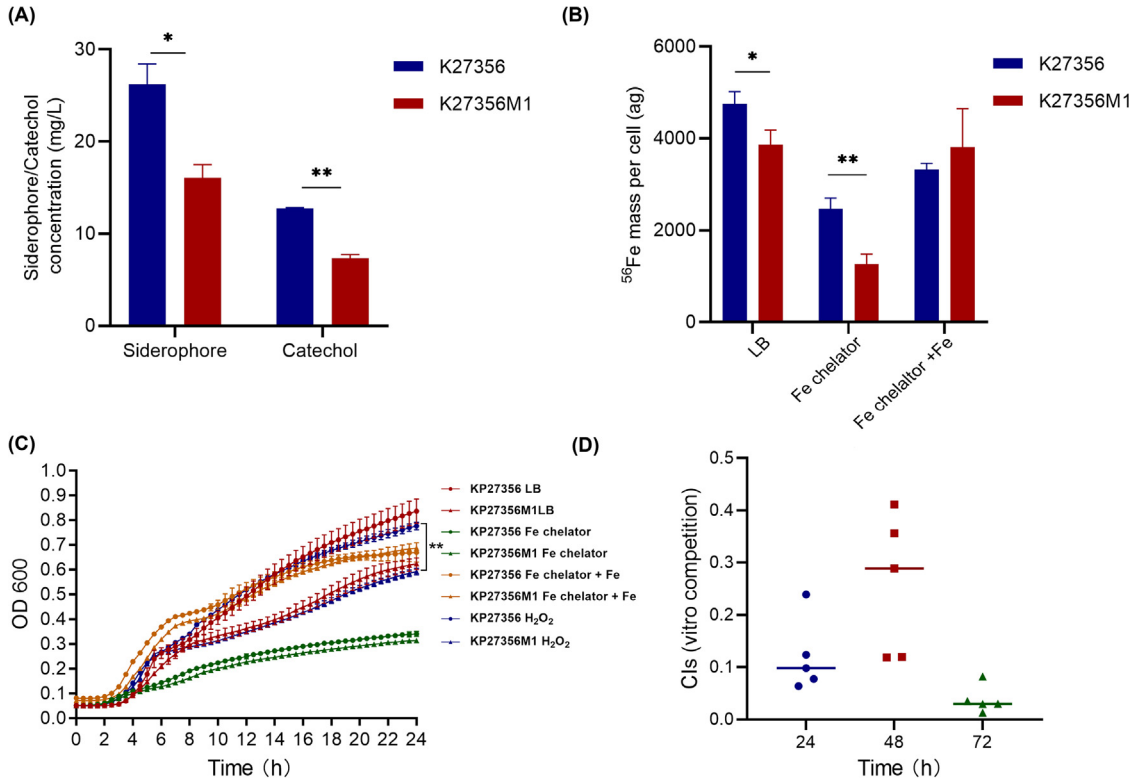

Fig. 5. General changes of K27356M1 after cefiderocol induction. (A) Quantitative detection of siderophores and catechol production of K27356 and K27356M1. (B) Quantitative detection of ^{56}Fe mass per bacteria in different iron content environments. (C) Growth curve of the WT strain and the cefiderocol-treated strain in different media. (D) Comparison of *in vitro* competitive ability between the WT and cefiderocol-treated strain.

whereas there were no significant differences between them under iron-sufficient (LB medium) ($P = 0.19$) and iron-deficient (Fe chelator) ($P = 0.39$) conditions, but exogenous iron rescued these phenotypes (Figure 5C). The competitive indexes (CIs) for the parent and mutant strain at 24, 48, and 72 h were 0.12, 0.26, and 0.038, respectively. The CIs for the K27356M1 were all well below 1, showing that the WT strains easily outcompeted the mutant strain (Figure 5D). All the changes observed above indicated that the acquisition of resistance comes at some expense of fitness.

3.6. The gain of cefiderocol resistance impaired the antioxidant capacity and survival ability in macrophages of K27356M1

The ability of pathogens to obtain iron from the host is central to their survival in macrophages [47]. Furthermore, genes *cysAT* are on the assimilatory sulfate reduction pathway, which has been linked to sulfur metabolism and macrophage antioxidant defense/adaptation [42]. Therefore, the ability to resist oxidative stress was detected. As displayed in Fig. 5C, there was a significant difference between the parental strain and the cefiderocol-treated strain in LB under the pressure of 0.5 mM H_2O_2 pressure ($P < 0.01$).

We then compared the phagocytosis ability and survival ability in macrophages between the parental strain and the mutant. As shown in Fig. 6A, the phagocytosis by RAW264.7 of K27356M1 was lower than that of K27356 with different co-incubation times. When the bacteria and cells were co-incubated for 2, 4, and 6 hours, there was a noticeable change. Additionally, an intracellular survival study was carried out (Fig. 6B). The difference in the CFU of survival bacteria between strains K27356 and K27356M1 at the point of 6 hours was statistically significant ($P<0.05$). Additionally, the phagocytosis by RAW 264.7 after 2 hours of co-incubation was observed by Confocal Laser Scanning Microscopy (CLSM). The average number of intracellular parental bacteria ingested by macrophages was higher than that of the mutant (Figure 6C, D). These results indicated that the cefiderocol-treated strain K27356M1 exhibits diminished resistance to macrophage phagocytosis due to impaired antioxidant capacity and iron acquisition.

4. Discussion

In clinical practice at present, the resistance to cefiderocol is mainly caused by the production of β-lactamase enzymes, and the combination of PER and NDM is a significant factor resulting in cefiderocol resistance [48]. Cefiderocol exhibits enhanced effectiveness against KPC-producing *K. pneumoniae* compared to NDM-producing strains [15]. Notably, our prior work challenged this paradigm by identifying cefiderocol resistance in multiple KPC-producing CR-hvKp [19]. Subsequent studies further revealed resistance driven by *cirA* mutations co-occurring with KPC-2/SHV-12 co-production [20] or through KPC-31 variants synergising with *fec* cluster-harbouring plasmids [21]. Nevertheless, these mechanisms are not sufficient to comprehensively account for resistance in strains without metallo-β-lactamases or typical siderophore defects.

This study aims to explore a previously unrecognised mechanism of cefiderocol resistance in KPC-producing ST11-KL64 CR-hvKP through the *in vitro* induction experiments. The *envZ* (V145G) mutation, identified across all resistant mutants, likely stabilises the kinase's active conformation, as evidenced by MIC reversion in K27356M1envZ^{G145V}, K27356M1ΔenvZ, and K27356ΔenvZ, as well as MIC increase in K27356envZ^{V145G}. In addition, the K27356M2 mutant carrying a concurrent *baeS* (V295G) mutation exhibited a higher cefiderocol MIC (512 μg/mL), suggesting that BaeS may act synergistically with EnvZ to further enhance resistance, consistent with previous reports in *Acinetobacter baumannii* [24].

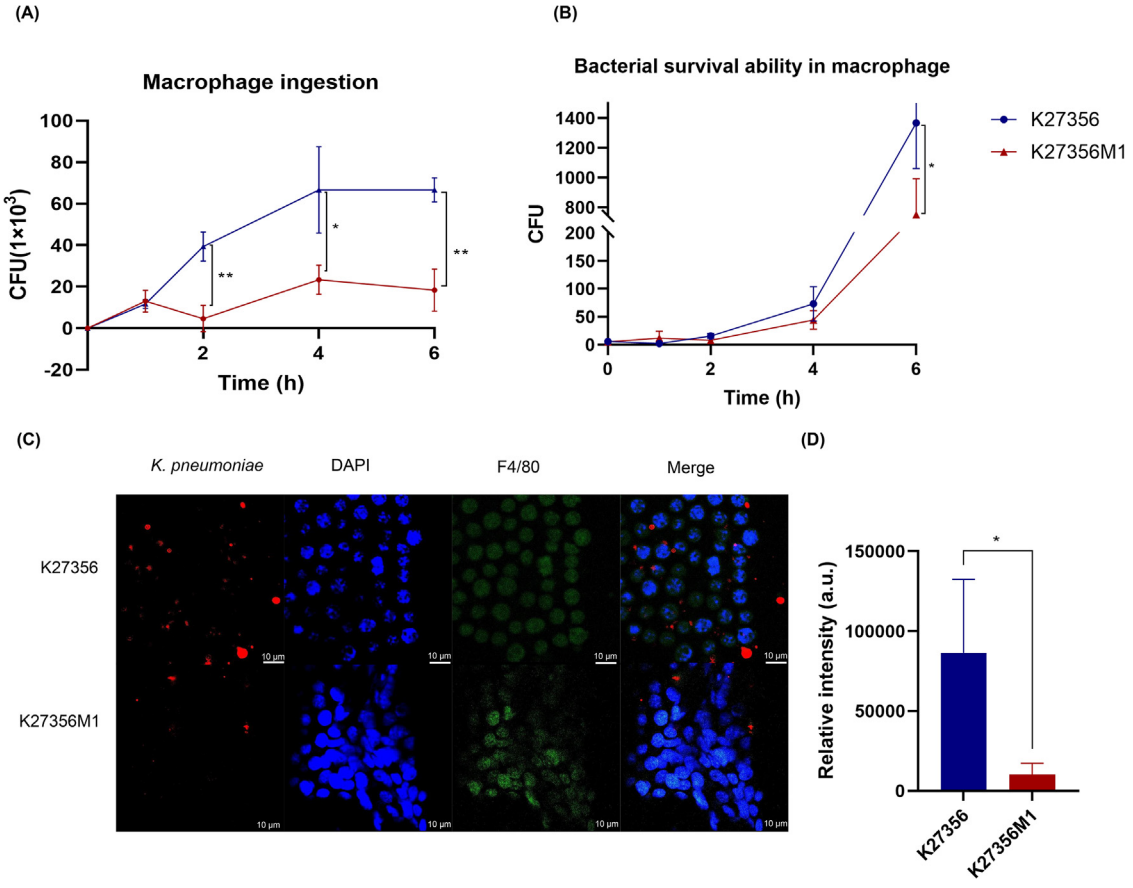

Fig. 6. Survival capability in macrophages between K27356 and K27356M1. Macrophage ingestion (A) and survival ability in macrophages (B) between K27356 and K27356M1. (C and D) The phagocytosis by RAW 264.7 of bacteria was observed by CLSM. The images of the multi-channel were merged by NIS Elements software, and the scale bar = 10 μm. Three replicates were performed.

Transcriptomic and proteomic data further revealed significant downregulation of iron acquisition pathways in mutant strain K27356M1, including the TonB-dependent transport system that also mediates cefiderocol import [8]. qRT-PCR confirmed that catecholate siderophore receptor and biosynthesis genes are downregulated by *envZ* (V145G), consistent with previous reports [9]. While the inactivation of the TonB energy-transducing system constitutes a stable downstream adaptation not readily reversed by *envZ* complementation. Because of the aforementioned modifications, the concentration of cefiderocol in the periplasm is reduced, allowing KPC-2 to hydrolyze cefiderocol. By overexpressing the above related genes (*fepA, cirA, entB, tonB*), we confirmed that the repression of catecholate siderophore transporters and the TonB complex leads to cefiderocol resistance synergistically. However, overexpressing *entB* can decrease cefiderocol's MIC, suggesting competitive uptake between cefiderocol and enterobactin via overlapping receptors [10,13]. In addition to directly repressing iron uptake-related genes, mutation in *envZ* can also indirectly activate *fur* by elevating intracellular Fe^{2+} iron levels, forming an active Fur–Fe^{2+} complex that strongly represses iron uptake genes [9]. Although *fur* was not activated, which may be due to the severely compromised iron acquisition ability, knocking out *fur* revealed that the resulting strain could also become more sensitive to cefiderocol by losing its repression of iron acquisition genes. Furthermore, the resistance phenotype may also be linked to the downregulation of ABC transporters, which needs further investigation.

The ability of pathogens to acquire iron from the host is critical for survival within macrophages [47]. As *cysAT* are essential for sulfate assimilation and glutathione biosynthesis, which is also a crucial antioxidant that may shield cells from oxidative stress and scavenge free radicals in the body [42]. Therefore, the repression of antioxidant ability and iron acquisition may render mutants susceptible to macrophage killing. The trade-off between resistance and fitness underscores an evolutionary dilemma for CR-hvKp: while mutations enhance antibiotic survival, they simultaneously reduce fitness in host environments.

Clinically, our results suggest dual therapeutic opportunities. First, the iron dependency of resistance implies that iron chelation (e.g., deferoxamine) could enhance cefiderocol efficacy, as supported by exogenous iron rescuing mutant growth. Second, the fitness costs may limit resistance dissemination in the absence of antibiotic pressure, offering avenues for resistance mitigation strategies. However, the study has some limitations. First, our reliance on *in vitro*-evolved mutants necessitates that these findings be validated in a broader collection of clinical isolates. Second, the precise regulatory cascade connecting the *envZ* mutation to the downregulation of iron transport genes remains to be fully elucidated. Future work should explore the potential synergistic contribution of the *baeS* (V295G) mutation to high-level resistance. The observed resistance may also involve downregulation of ABC transporters, warranting further investigation. Expanding the analysis to additional clinical isolates will be essential to fully elucidate the complex interplay of these genes in cefiderocol resistance. Furthermore, the fitness trade-offs identified here should be assessed *in vivo* using appropriate murine infection models to confirm their clinical relevance.

In conclusion, we report a KPC-producing ST11-KL64 cefiderocol-resistant CR-hvKp strain harbouring an amino acid

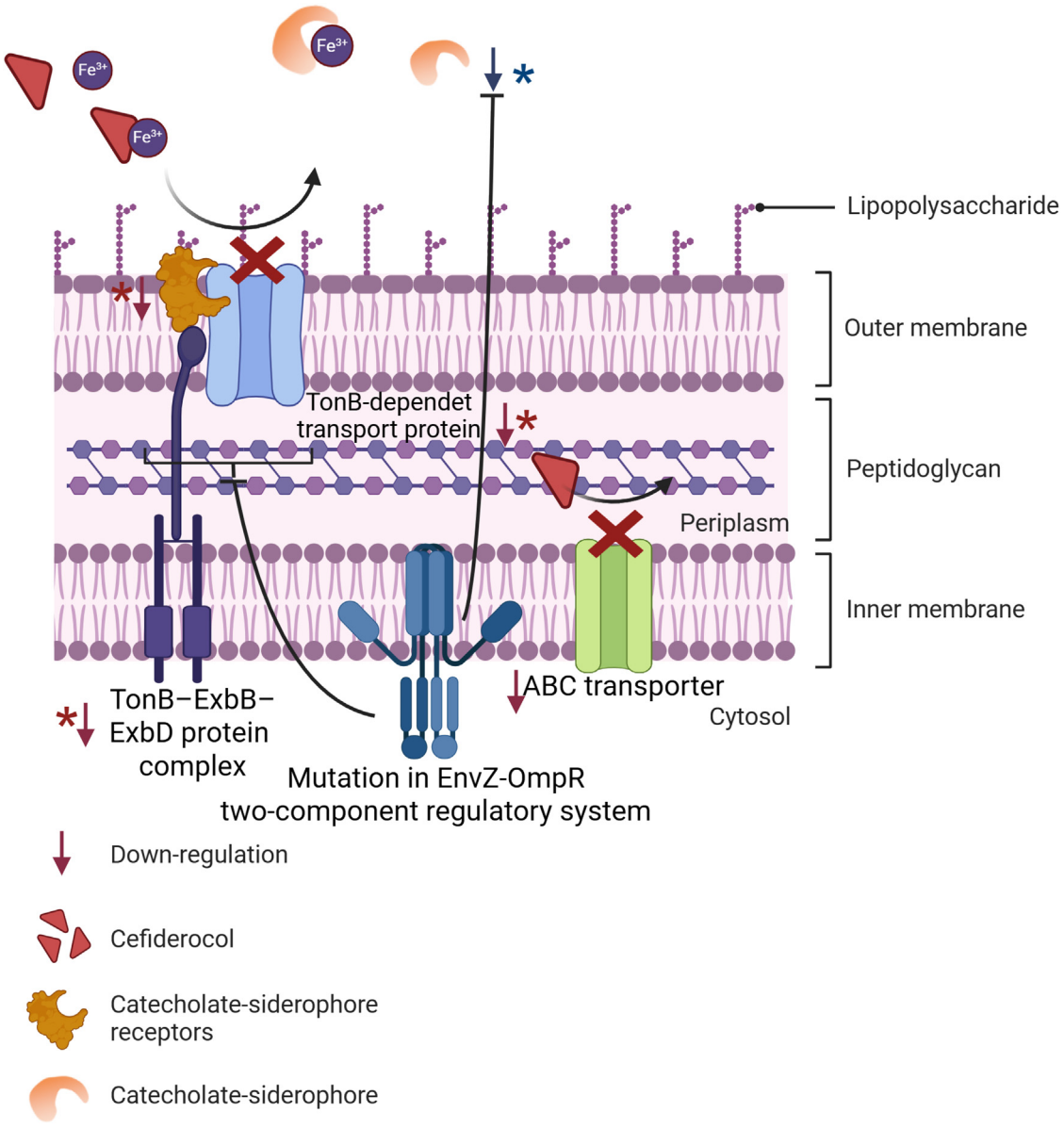

Fig. 7. Proposed mechanisms of cefiderocol resistance in K3756M1. Various disruptions at key stages of the cefiderocol entry and action within the bacterial envelope may result in resistance (shown in red), including dysregulation of catecholate siderophore receptors resulting from a mutation in the EnvZ–OmpR TCS (*envZ* (V145G)), TonB-ExbB-ExbD, and ABC transporters. Suppression of enterobactin biosynthesis attenuates this resistance phenotype (shown in blue). Resistance mechanisms confirmed in this study are indicated with an asterisk (created with BioRender.com).

substitution in *envZ*, which led to downregulation of siderophore transporter proteins, together with downregulation of the TonB-ExbB-ExbD energy-transducing complex (Fig. 7). This disruption impairs the "Trojan horse" mechanism that cefiderocol exploits to accumulate in the bacterial periplasm, resulting in high-level cefiderocol resistance and reduced bacterial fitness. This resistance mechanism can be strengthened by *baeS* mutation and upregulation of catecholate siderophore synthesis *entB*. The downregulated ABC transporters identified in the combined transcriptomic-proteomic analysis may also contribute to cefiderocol resistance. As far as we are aware, this is the first description of an *in vitro* induced KPC-producing CR-hvKp strain exhibiting high-level resistance to cefiderocol (MIC = 256 μg/mL), which may provide insights into potential mechanisms of cefiderocol resistance. Even though cefiderocol has not yet been approved in China, it is crucial to raise awareness and launch coordinated efforts to control this new superbug.

Declarations

Funding: This study was supported by the Horizontal research project of China-Japan Friendship Hospital [2024-HX-JC-22], Elite Medical Professionals Project of China-Japan Friendship Hospital [ZRJY2023-QM32], National Natural Science Foundation of China (NSFC) [82102456], and the Chinese Academy of Medical Sciences (CAMS) Innovation Fund for Medical Sciences [CIFMS 2021-I2M-1-048].

Ethical approval: This study was approved by the Ethics Committee of China-Japan Friendship Hospital (2022-KY-054).

Sequence information: The sequence of strain K27356 was deposited in the GenBank SRA database (Bioproject: PRJNA1229757; accession numbers of isolates: SRR32638446).

Declaration of competing interests: None declared.

Supplementary materials

Supplementary material associated with this article can be found, in the online version, at doi:10.1016/j.ijantimicag.2025.107693.

References

[1] Lan P, Jiang Y, Zhou J, Yu Y. A global perspective on the convergence of hypervirulence and carbapenem resistance in Klebsiella pneumoniae. J Glob Antimicrob Resist 2021;25:26–34.
[2] Lai YC, Lu MC, Hsueh PR. Hypervirulence and carbapenem resistance: two distinct evolutionary directions that led high-risk Klebsiella pneumoniae clones to epidemic success. Expert Rev Mol Diagn 2019;19(9):825–37.
[3] Martin RM, Bachman MA. Colonization, infection, and the accessory genome of Klebsiella pneumoniae. Front Cell Infect Microbiol 2018;8:4.
[4] Lasko MJ, Nicolau DP. Carbapenem-resistant enterobacterales: considerations for treatment in the era of new antimicrobials and evolving enzymology. Curr Infect Dis Rep 2020;22(3):6.
[5] Russo TA, Marr CM. Hypervirulent Klebsiella pneumoniae. Clin Microbiol Rev 2019;32(3):e00001–19.
[6] Pu D, Zhao J, Chang K, Zhuo X, Cao B. Superbugs" with hypervirulence and carbapenem resistance in Klebsiella pneumoniae: the rise of such emerging nosocomial pathogens in China. Sci Bull (Beijing) 2023;68(21):2658–70.
[7] Sato T, Yamawaki K. Cefiderocol: discovery, chemistry, and In vivo profiles of a novel siderophore cephalosporin. Clin Infect Dis 2019;69(Suppl 7):S538–43.
[8] Wang L, Zhu J, Chen L, Du H, et al. Cefiderocol: clinical application and emergence of resistance. Drug Resist Updat 2024;72:101034.
[9] Gerken H, Vuong P, Soparkar K, Misra R. Roles of the EnvZ/OmpR two–component system and porins in iron acquisition in Escherichia coli. mBio 2020;11(3):e01192-20.
[10] Oshima T, Aiba H, Masuda Y, Kanaya S, Sugiura M, Wanner BL, et al. Transcriptome analysis of all two-component regulatory system mutants of Escherichia coli K-12. Mol Microbiol 2002;46(1):281–91.
[11] Yamano Y, Nakamura R, Takemura M, Echols R. Potential mechanisms of cefiderocol MIC increase in enterobacterales in In vitro resistance acquisition studies. Open Forum Infect Dis 2020;7:S730.
[12] Findlay J, Bianco G, Boattini M, Nordmann P. High-level cefiderocol and ceftazidime/avibactam resistance in KPC-producing Klebsiella pneumoniae associated with mutations in KPC and the sensor histidine kinase EnvZ. J Antimicrob Chemother 2025;80(4):1155–7.
[13] Han R, Niu M, Liu S, Mao J, Yu Y, Du Y. The effect of siderophore virulence genes entB and ybtS on the virulence of carbapenem-resistant Klebsiella pneumoniae. Microb Pathog 2022;171:105746.
[14] Padovani M, Bertelli A, Corbellini S, Piccinelli G, Gurrieri F, De Francesco MA. In vitro activity of cefiderocol on multiresistant bacterial strains and genomic analysis of two cefiderocol resistant strains. Antibiotics (Basel) 2023;12(4):785.
[15] Kazmierczak KM, Tsuji M, Wise MG, Hackel M, Yamano Y, Echols R, et al. In vitro activity of cefiderocol, a siderophore cephalosporin, against a recent collection of clinically relevant carbapenem-non-susceptible gram-negative bacilli, including serine carbapenemase- and metallo-β-lactamase-producing isolates (SIDERO-WT-2014 Study). Int J Antimicrob Agents 2019;53(2):177–84.
[16] Lan P, Lu Y, Jiang Y, Wu X, Yu Y, Zhou J. Catecholate siderophore receptor CirA impacts cefiderocol susceptibility in Klebsiella pneumoniae. Int J Antimicrob Agents 2022;60(4):106646.
[17] Wang Q, Jin L, Sun S, Yin Y, Wang R, Chen F, et al. Occurrence of high levels of cefiderocol resistance in carbapenem-resistant Escherichia coli before its approval in China: a report from China CRE-Network. Microbiol Spectr 2022;10(3):e0267021.
[18] Lan P, Lu Y, Chen Z, Wu X, Hua X, Jiang Y, et al. Emergence of high-level cefiderocol resistance in carbapenem-resistant Klebsiella pneumoniae from bloodstream infections in patients with hematologic malignancies in China. Microbiol Spectr 2022;10(2):e0008422.
[19] Zhao J, Pu D, Li Z, Liu X, Zhang Y, Wu Y, et al. In vitro activity of cefiderocol, a siderophore cephalosporin, against carbapenem-resistant hypervirulent Klebsiella pneumoniae in China. Antimicrob Agents Chemother 2023;67(12):e0073523.
[20] Lan P, Lu Y, Liao W, Yu Y, Fu Y, Zhou J. Cefiderocol-resistant hypervirulent Klebsiella pneumoniae with CirA deficiency and co-production of KPC-2 and SHV-12. Clin Microbiol Infect 2025;31(1):125–7.
[21] Polani R, De Francesco A, Tomolillo D, Artuso I, Equestre M, Trirocco R, et al. Cefiderocol resistance conferred by Plasmid-located ferric citrate transport system in KPC-producing Klebsiella pneumoniae. Emerg Infect Dis 2025;31(1):123–4.
[22] Pu D, Zhao J, Lu B, Zhang Y, Wu Y, Li Z, et al. Within-host resistance evolution of a fatal ST11 hypervirulent carbapenem-resistant Klebsiella pneumoniae. Int J Antimicrob Agents 2023;61(4):106747.
[23] Institute CaLS. Performance standards for antimicrobial susceptibility testing. CLSI supplement M100. 32nd ed. Wayne, PA: Clin. Lab. Stand. Inst; 2022.
[24] Liu X, Chang Y, Xu Q, Zhang W, Huang Z, Zhang L, et al. Mutation in the two–component regulator BaeSR mediates cefiderocol resistance and enhances virulence in Acinetobacter baumannii. mSystems 2023;8(4):e0129122.
[25] Jiang H, Lei R, Ding SW, Zhu S. Skewer: a fast and accurate adapter trimmer for next-generation sequencing paired-end reads. BMC Bioinformatics 2014;15:182.
[26] Bankevich A, Nurk S, Antipov D, Gurevich AA, Dvorkin M, Kulikov AS, et al. SPAdes: a new genome assembly algorithm and its applications to single-cell sequencing. J Comput Biol 2012;19(5):455–77.
[27] Wick RR, Judd LM, Gorrie CL, Holt KE. Unicycler: resolving bacterial genome assemblies from short and long sequencing reads. PLoS Comput Biol 2017;13(6):e1005595.
[28] Seemann T. Prokka: rapid prokaryotic genome annotation. Bioinformatics 2014;30(14):2068–9.
[29] Lam MMC, Wick RR, Watts SC, Cerdeira LT, Wyres KL, Holt KE. A genomic surveillance framework and genotyping tool for Klebsiella pneumoniae and its related species complex. Nat Commun 2021;12(1):4188.
[30] Barrick JE, Colburn G, Deatherage DE. Identifying structural variation in haploid microbial genomes from short-read resequencing data using breseq. BMC Genomics 2014;15(1):1039.
[31] McClure R, Balasubramanian D, Sun Y, Bobrovskyy M, Sumby P, Genco CA, et al. Computational analysis of bacterial RNA-seq data. Nucleic Acids Res 2013;41(14):e140.
[32] McCarthy DJ, Chen Y, Smyth GK. Differential expression analysis of multifactor RNA-seq experiments with respect to biological variation. Nucleic Acids Res 2012;40(10):4288–97.
[33] Liao Y, Smyth GK, Shi W. FeatureCounts: an efficient general purpose program for assigning sequence reads to genomic features. Bioinformatics 2014;30(7):923–30.
[34] Love MI, Huber W, Anders S. Moderated estimation of fold change and dispersion for RNA-seq data with DESeq2. Genome Biol 2014;15(12):550.
[35] Ma C, Wang W, Wang Y, Sun Y, Kang L, Zhang Q, et al. TMT-labeled quantitative proteomic analyses on the longissimus dorsi to identify the proteins underlying intramuscular fat content in pigs. J Proteomics 2020;213:103630.
[36] Sun M, Liu Y, Song Y, Gao Y, Zhao F, Luo Y, et al. The ameliorative effect of Lactobacillus plantarum-12 on DSS-induced murine colitis. Food Funct 2020;11(6):5205–22.
[37] Cox J, Mann M. MaxQuant enables high peptide identification rates, individualized p.p.b.-range mass accuracies and proteome-wide protein quantification. Nat Biotechnol 2008;26(12):1367–72.
[38] Russo TA, MacDonald U, Hassan S, Camanzo E, LeBreton F, Corey B, et al. An assessment of siderophore production, mucoviscosity, and mouse infection models for defining the virulence spectrum of hypervirulent Klebsiella pneumoniae. mSphere 2021;6(2):e00045-21.
[39] Bulger J, MacDonald U, Olson R, Beanan J, Russo TA. Metabolite transporter PEG344 is required for full virulence of hypervirulent Klebsiella pneumoniae strain hvKP1 after pulmonary but not subcutaneous challenge. Infect Immun 2017;85(10):e00093-17.
[40] Russo TA, Olson R, Macdonald U, Metzger D, Maltese LM, Drake EJ, et al. Aerobactin mediates virulence and accounts for increased siderophore production under iron-limiting conditions by hypervirulent (hypermucoviscous) Klebsiella pneumoniae. Infect Immun 2014;82(6):2356–67.
[41] Arnow LE. Colorimetric determination of the components of 3,4-dihydroxyphenylalaninetyrosine mixtures. J Biol Chem 1937;118(2):531–7.
[42] Jia X, Zhu Y, Jia P, Li C, Chu X, Sun T, et al. The key role of iroBCDN-lacking pLVPK-like plasmid in the evolution of the most prevalent hypervirulent carbapenem-resistant ST11-KL64 Klebsiella pneumoniae in China. Drug Resist Updat 2024;77:101137.
[43] Panjaitan NSD, Horng YT, Chien CC, Yang HC, You RI, Soo PC. The PTS components in Klebsiella pneumoniae affect bacterial capsular polysaccharide production and macrophage phagocytosis resistance. Microorganisms 2021;9(2):335.
[44] Giner G, Smyth GK. Statmod: probability calculations for the inverse gaussian distribution. R Journal 2016;8:339–51.
[45] Roichman A, Elhanati S, Aon MA, Abramovich I, Di Francesco A, Shahar Y, et al. Restoration of energy homeostasis by SIRT6 extends healthy lifespan. Nat Commun 2021;12(1):3208.
[46] Nairz M, Weiss G. Iron in infection and immunity. Mol Aspects Med 2020;75:100864.
[47] Wang H, Xu Q, Zhao W, Chan BKW, Chen K, Xie M, et al. Simultaneous functional disruption of the iron acquisition system and type VI secretion system results in complete suppression of virulence in Acinetobacter baumannii. Microbiol Res 2025;295:128105.
[48] Ito A, Hackel M, Sahm DF, Tsuji M, Yamano Y. Characterization of isolates showing high MICs to cefiderocol from global surveillance study SIDERO-CR-2014/2016. In: the 29th European Congress of Clinical Microbiology and Infectious Diseases; 2019. p. 13–16.